Decoding the Oral Microbiome: Metagenomic Insights into Host Metabolic Health

Haochen Xue[1,3], Anastasia Godneva[2], Feilong Tang[1], Huifa Li[1], Yulong Li[1], Ming Hu[1], Ruobing Li[3], Jionglong Su[3], Eran Segal[1,2†], Imran Razzak[1†]

[1]Mohamed bin Zayed University of Artificial Intelligence, UAE.
[2]Weizmann Institute of Science, Israel.
[3]University of Liverpool, UK.

[†]Corresponding authors: {Eran.Segal, Imran.Razzak}@mbzuai.ac.ae;

Abstract

The oral microbiome may capture system-specific information about host metabolic health, yet large-scale, multi-system evidence remains scarce. We analyzed 9,431 participants in the Human Phenotype Project (HPP), integrating oral whole-metagenome profiles with 44 metabolic measures spanning liver ultrasound, continuous glucose monitoring (CGM), and dual-energy X-ray absorptiometry (DXA). A multilayer map across strains, gene families and pathways revealed widespread associations: 213 strains, 124,603 gene families and 299 pathways were significantly associated with metabolic measures. Prioritizing the strongest and cross-phenotype signals, we identified multiple oral features that exhibit multifaceted and significant associations with metabolic health. For example, acyl carrier protein (ACP) associated with lower liver inflammation and reduced adiposity, whereas polyamine biosynthesis and ceramide α-oxidation tracked higher glucose variability and adverse liver and adiposity phenotypes. We further trained disease prediction models using only oral features that were significantly associated with the clinical phenotypes of each disease; compared with models using the full feature set, these models consistently achieved higher performance across six metabolic diseases. Together, these findings provide reproducible evidence for future research and highlight the potential of oral microbial markers as non-invasive tools for metabolic risk stratification and as promising targets for microbiome-based interventions in metabolic diseases.

Keywords: Oral microbiome, Population-scale cohort, Strain-resolved metagenomics, Microbial gene families and pathways, Multi-system phenotypes, Metabolic health

1 Introduction

The oral microbiome is a complex and dynamic ecosystem at the interface between the host and the environment, playing a vital role in maintaining both oral and systemic health [1–3]. Beyond its well-established involvement in caries and periodontitis [4, 5], oral dysbiosis has been linked to implicated in cardiovascular, autoimmune, and metabolic disorders [6, 7]. Mounting evidence links alterations in the oral microbiome to metabolic conditions such as non-alcoholic fatty liver disease (NAFLD), type 2 diabetes, and obesity [8, 9]. Clinical and experimental studies further support the links between the oral microbiome and metabolic diseases. In liver disease, reduced oral microbial diversity and enrichment of genera such as Streptococcus, Porphyromonas, and Actinomyces have been reported [10], while phylum-level compositional shifts characterize NAFLD [11]. Similarly, in disorders of glucose metabolism, increased abundance of opportunistic taxa has been observed in individuals with diabetes [12], with corresponding microbial alterations reproduced in diabetic mouse models [13]. Most of these findings are predominantly compositional and descriptive, and the functional mechanisms underlying these associations remain largely unexplored.

Despite the substantial progress in oral microbiome research, the mechanistic link between microbial function and host metabolic phenotypes remain poorly understood. Two major limitations have constrained advances (i) most of the existing studies rely on 16S rRNA gene profiling to assess microbial diversity and taxonomic composition in metabolically healthy versus diseased individualsl however, 16S rRNA sequencing [14] provides limited taxonomic resolution and does not directly capture microbial genes or functional pathways. Consequently, the contributions of specific strains, gene families, and metabolic functions remain largely unresolved, obscuring causal links to host metabolic phenotypes. (ii) recent studies are statistically underpowered due to small sample sizes and the prevalent use of binary case–control designs focused on single diseases. This narrow framework overlooks the complex, multisystem nature of metabolic health, limiting the biological and clinical relevance of current findings.

In this study, we address the gaps mentioned above by using the Human Phenotype Project (HPP), a large-scale longitudinal deep-phenotyping cohort of 9,431 individuals [15]. Using metagenomic profiling (MetaPhlAn4 and HUMAnN3), we profiled oral metagenomes and analyzed microbial features across strains, gene families, and pathways. Furthermore, HPP used advanced techniques to collect a wide array of multi-organ metabolic health phenotypes, including liver status via liver ultrasound, dynamic glucose homeostasis via continuous glucose monitoring (CGM), and visceral adipose tissue via dual-energy X-ray absorptiometry (DXA). Building on these large-scale and high-dimensional data, we developed a framework similar to Genome-Wide Association Study (GWAS) [16] to systematically investigate associations between oral microbial features and host metabolic phenotypes. This study provides a phenotype-resolved view of how the oral microbiome relates to metabolic health and a resource for mechanistic studies and risk stratification.

2 Results

2.1 Study design and research population

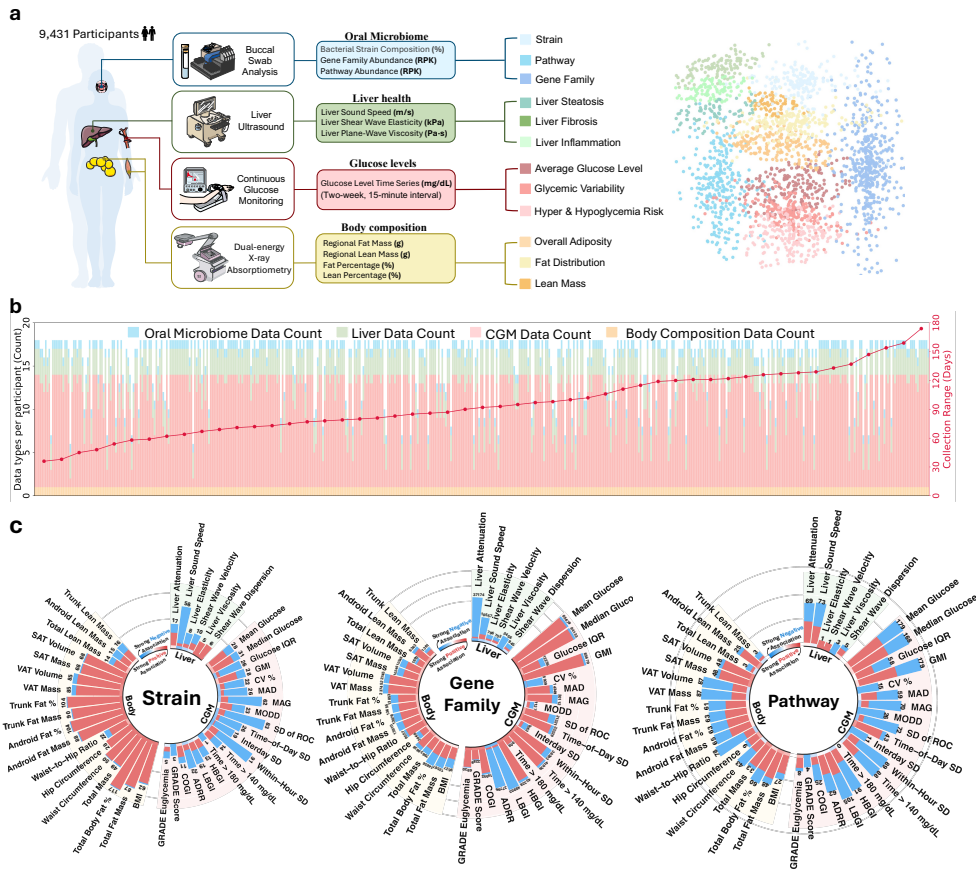

Fig. 1: **a**, Data collected in the Human Phenotype Project (HPP; n = 9,431): oral metagenomes (strains, gene-family, and pathway), liver ultrasound (sound speed, elasticity, viscosity), continuous glucose monitoring (CGM; 15-min over 14 days), and dual-energy X-ray absorptiometry (DXA; body composition). Right: two-dimensional embedding of the 44 phenotypes, colored by physiological system. **b**, Coverage and timing for a random sample of 500 participants. Stacked bars show modality-specific phenotype counts; the red line is each participant's collection span (days). Association analyses in Methods 4.4 used the full cohort and a 180-day window. **c**, Significant associations between oral microbial features and the 44 phenotypes at three levels (strain, gene family, pathway). Radial bars show counts per phenotype; colors indicate direction (red, positive; blue, negative). Significance: Bonferroni-corrected $P < 0.05$.

Table 1: Summary statistics of key metabolic phenotypes, the full list and extended statistics are provided in Supplementary Table S1.

Metabolic Phenotype		**Male n=4474(47.4%)**	**Female n=4957(52.6%)**
Age		55.49 (7.95)	56.24 (8.01)
Liver Health			
Liver Steatosis	Liver sound speed (m/s)	1547.36 (23.07)	1539.51 (23.69)
	Liver attenuation (dB/cm/MHz)	0.41 (0.10)	0.41 (0.10)
Fibrosis	Liver Elasticity (kPa)	5.43 (1.25)	4.68 (0.94)
	Shear Wave Velocity (m/s)	1.34 (0.14)	1.24 (0.12)
Inflammation	Liver Viscosity (Pa·s)	1.70 (0.24)	1.62 (0.27)
	Shear Wave Dispersion ((m/s)/kHz)	2.46 (0.45)	2.32 (0.50)
Glycemic Control (CGM)			
Average Glucose Level	Mean Glucose (mg/dL)	97.35 (13.74)	94.08 (11.23)
	Glucose Management Indicator (GMI, %)	5.64 (0.33)	5.56 (0.27)
Glycemic Variability	Coefficient of Variation (CV, %)	15.95 (4.18)	16.15 (4.00)
	Mean of Daily Differences (MODD, mg/dL)	13.62 (4.93)	12.88 (4.04)
Hyper/Hypoglycemia Risk	High Blood Glucose Index (HBGI)	0.23 (0.94)	0.14 (0.36)
	Low Blood Glucose Index (LBGI)	2.18 (1.91)	2.57 (1.94)
Glycemic Control Quality	Composite Glycemic Index (COGI)	0.89 (0.16)	0.86 (0.17)
	Diabetes Risk Assessment Equation (GRADE)	1.37 (1.23)	1.24 (0.85)
Body Composition			
Overall Adiposity	Total Fat Mass (kg)	23.16 (8.05)	25.98 (8.56)
	Total Body Fat (%)	28.52 (6.32)	38.71 (6.79)
Fat Distribution	Android Fat Mass (g)	2327.65 (1105.68)	2071.05 (963.79)
	VAT Mass (g)	1211.70 (748.66)	647.77 (458.77)
Lean Mass	Total Lean Mass (kg)	56.33 (6.82)	39.67 (4.98)
	Android Lean Mass (kg)	4.07 (0.57)	2.90 (0.43)

The Human Phenotype Project cohort includes 9,431 participants with available data on the oral microbiome and metabolic phenotypes. We collected liver metabolic health data using liver ultrasound, continuous glucose levels via CGM, and whole body fat data through DXA. Data modalities are summarised in Fig. 1a, and Fig. 1b illustrates per-participant coverage and the sampling window. The summary statistics for key metabolic phenotypes are shown in Table 1, and detailed collection methods are described in Methods 4.3.

To ensure data reliability, liver ultrasound was measured three times in a single day, and the average value was used for analysis. For CGM, interstitial fluid glucose levels were continuously monitored for two weeks, with readings taken every 15 minutes. For body composition data, 94.25% of participants had a single DXA measurement. For the 5.75% with multiple measurements (with time intervals ranging from 3 days to 22 months), data were processed in relation to the collection date of the oral microbiome sample. Specifically, if all of a participant's DXA measurements fell within six months before or after their microbiome sample collection, the average of these measurements was used. Furthermore, for the correlation analysis, only metabolic phenotype data

(liver ultrasound, CGM and DXA) collected within a six-month window centred on the oral-swab date were included.

Oral microbiome data were processed using MetaPhlAn 4 and HUMAnN 3.6 to characterize the taxonomic composition and functional potential. MetaPhlAn 4 provided the relative abundance of microbial taxa at all levels, from kingdom to strain. Subsequently, the abundance of gene families and pathways was quantified by HUMAnN 3.6 to reflect the functional profile of the microbial community. For subsequent correlation analysis, we used preprocessed strain-level abundances from MetaPhlAn 4 and functional data on gene families and pathways from HUMAnN 3.6, details in Methods 4.2.

2.2 System-specific oral microbiome associations with metabolic phenotypes

Across 44 host phenotypes spanning liver, continuous glucose monitoring, and body composition, we analyzed 783 bacterial strains, 355,674 gene families, and 786 pathways. Among these, 213 strains (27.20%), 124,603 gene families (35.03%), and 299 pathways (38.04%) showed significant associations with at least one phenotype (Fig. 1c). Across all oral microbiome feature–phenotype pairs, positive associations predominated for strains (70.76%) and gene families (72.79%), whereas pathways exhibited a nearly balanced distribution (49.29% positive). Beyond these overall counts, two key patterns emerged. First, we observed extensive pleiotropy: most oral microbial features were linked to more than one host phenotype (90.20% of strains, 90.54% of gene families, and 94.98% of pathways). Second, we identified clear system-level specificity, with roughly half of the features (50.23% of strains, 59.29% of gene families, and 44.82% of pathways) showing associations restricted to a single metabolic domain—liver, CGM, or body composition. This coexistence of broad pleiotropy and system-level specificity formed the foundation for subsequent system-focused analyses.

Similarly, body composition exhibited the highest number of significant associations with strain at the system level, accounting for 63.68% of all significant strain–phenotype associations, compared to 30.57% for CGM-strain and 5.75% for the strain–liver associations. Furthermore, body also showed the highest association density, with a mean of 64.00% strains per phenotype, exceeding both liver (17.33%) and CGM (27.74%). Specifically, 46 strains were uniquely associated with body composition phenotypes and showed no significant associations with other systems. Among significant body–strain associations, positive relationships dominated (94.79%). Within body composition phenotypes, Total Body Fat% displayed the highest degree of association, with 117 strains significantly linked, of which 98.29% were positively associated. This positive dominant pattern was prevalent in all fat-related phenotypes: for measures of overall adiposity (e.g., BMI, Total Fat Mass), the mean proportion of positive associations was 96.62%; for indicators of fat distribution (e.g., Android Fat Mass, Trunk Fat Mass), the mean was 95.94%. A similar but attenuated trend was observed for the lean mass–related phenotypes, where the proportion of positive associations decreased to 60%. These results indicate that the strength of positive strain–host associations is strongly phenotype-dependent, being more pronounced for fat-related phenotypes than for lean mass.

At the functional level—encompassing gene families and pathways—the strongest associations shifted from body composition to CGM. Based on association counts, 70.20% of significant gene family associations and 57.41% of pathway associations were attributed to CGM. The CGM also exhibited the highest association density, with a mean of 29,951 significant associations per phenotype, exceeding body composition and liver (8,780 and 11,042, respectively). Moreover, the CGM also contained the largest number of system-specific signals, with 56,817 gene families and 107 pathways uniquely associated with CGM, markedly higher than the second-ranked body composition system (4,648 gene families and 16 pathways).

Given this strong system-specific enrichment, we next examined the directionality of CGM-associated features. Gene family associations were predominantly positive (78.66%), particularly for mean glucose and hyperglycemia metrics (95.34% positive), whereas hypoglycemia-weighted indices (LBGI, ADRR) were largely negative (4.13% positive). Within this overall positive framework, some divergence emerged among glycemic variability phenotypes: while most followed the positive trend, CV% exhibited far fewer associations and was overwhelmingly negative (1.97% positive). In comparison to gene families, CGM–pathway associations were more heterogeneous. For mean and median glucose, pathways mirrored gene-family directionality but with a lower positive fraction (61.38%). For variability phenotypes—including distributional (glucose IQR, CV%, MAD), short-term within-day (MAG, SD of ROC, within-hour SD), and between-day metrics (inter-day SD, MODD)—associations were predominantly negative, except for Time-of-Day SD, which remained largely positive (86.04%). This pattern aligns with the underlying metric definitions: Time-of-Day SD captures reproducible within-day glucose rhythms (e.g., pre-/post-prandial peaks, nocturnal troughs), whereas the other variability metrics primarily reflect stochastic short-term fluctuations or day-to-day instability. In contrast to CGM, the liver domain exhibited the fewest significant associations but showed clear pathology-specific patterns. For inflammation-related phenotypes, strain-level associations were uniformly positive, whereas pathway-level associations were predominantly negative (62.50%), with viscosity-related pathways being entirely negative. For fibrosis-related phenotypes, this directionality was reversed: strain-level associations were largely negative (66.67%), while both identified fibrosis-associated pathways ($n = 2$) showed positive associations. Together, these results indicate that, although the liver exhibited a lower overall association density, its microbial relationships were highly phenotype-specific and reflected distinct biological processes across inflammatory and fibrotic states.

To prioritize independent signals from the highly correlated oral gene families, we applied a two-step filtering strategy: a pre-association decorrelation filter applied before association testing, followed by post-association pruning based on the correlation structure (Methods 4.5). After pre-filtering and post-hoc clumping, the most robust and independent associations emerged for phenotypes reflecting overall glycemic status. For example, GMI retained 327 gene families after pre-filtering and 41 after clumping, while mean glucose retained 322 and 35, respectively—demonstrating substantial independence among signals. By contrast, certain phenotypes exhibited large unfiltered association counts but high redundancy. For instance, HBGI and LBGI were initially associated with 45,328 and 48,903 gene families, respectively; however,

post-clumping reduced these to just 29 and 26 independent signals, revealing extensive collinearity within their underlying association networks.

2.3 Most significant associated oral strains, gene families, and pathways

Our analyses (Results 2.2) identified extensive and statistically significant associations between oral microbial features and host metabolic phenotypes, including 213 strains, 124,603 gene families, and 299 pathways. To identify the most informative microbial units, we applied a systematic selection strategy (Methods 4.6), identifying 15 strains, 15 gene families, and 13 pathways as core markers of host metabolic health. The associations for these core markers are summarized in Figs. 2, 3, and 4.

Based on their cross-phenotype directions, we then grouped markers into three classifications: (1) Beneficial Profile, associated with improved metabolic health; (2) Detrimental Profile, associated with impaired metabolic health; and (3) Mixed Profile, associated with both beneficial and detrimental metabolic traits. Applying this same classification to all Bonferroni-significant features yielded the following distributions: strains, 50/105/58; gene families, 17,782/44,648/62,173; pathways, 77/71/151 (Beneficial/Detrimental/Mixed). The sections that follow examine the core strains, gene families, and pathways within each category in detail. To our knowledge, this represents one of the first cohort-scale maps of the oral microbiome that concurrently resolves strain-, gene family-, and pathway-level associations across multiple host metabolic systems. Given the relative scarcity of strain-level data in the oral microbiome literature, we contextualize our findings using species- or genus-level reports where available and draw on non-oral studies for shared microbial genes and pathways when oral evidence is lacking.

2.3.1 Significant strains

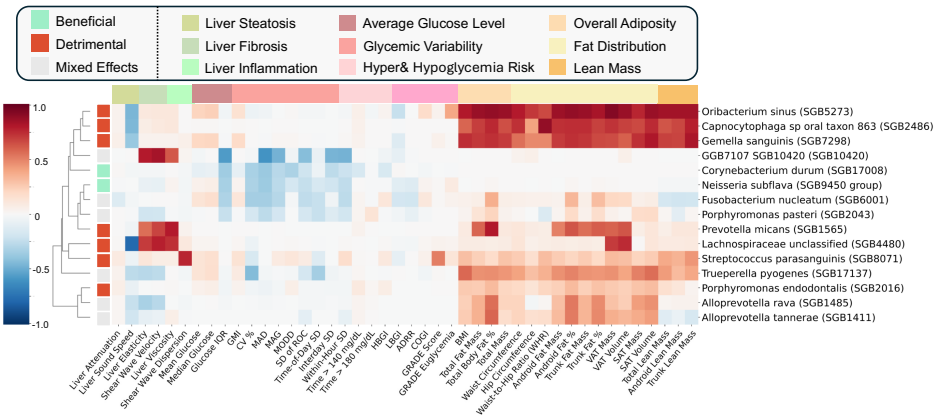

Fig. 2: Heatmap illustrating the associations between 15 core oral microbial strains and 44 metabolic phenotypes. The selection method is detailed in Methods 4.6.

Among 15 selected most significant strains, 2 strains showed a beneficial profile. Corynebacterium durum (SGB17008) associated with better glycemic control and lower CGM variability. Prior studies reported Corynebacterium durum (species-level) directionally concordant links to improved glycemic responses [9, 17]. Likewise, Neisseria subflava (SGB9450 cluster) was associated with more stable glucose and lower risk of hepatic inflammation and fibrosis, consistent with Neisseria subflava (species-level) identified as protective in metabolic dysfunction [18, 19].

In contrast, we also identified 7 detrimental strains. Oribacterium sinus (SGB5273) and Prevotella micans (SGB1565) aligned with worse liver health and higher glucose and greater total/visceral adiposity; Lachnospiraceae taxon (SGB4480) showed a similar liver profile with increased adiposity/weight; Capnocytophaga taxon 863 (SGB2486) marked hepatic and body adiposity without CGM associations. In the CGM-anchored subset, Gemella sanguinis (SGB7298), Streptococcus parasanguinis (SGB8071) and Porphyromonas endodontalis (SGB2016) aligned with higher glucose and CGM variability, also increased body adiposity and liver steatosis. Where higher-rank reports exist, directions are consistent: Oribacterium sinus (species-level) has been linked to inflammatory responses under high-fat diet conditions [20, 21]; Prevotella micans (species-level) has been associated with greater fibrosis severity in NAFLD [22]; Lachnospiraceae taxa (family-level) have been associated with advanced fibrosis, increased liver stiffness and deteriorated glycemic profiles in gut cohorts [23]; Capnocytophaga (genus-level) has been implicated in NAFLD via oral–gut translocation [24]; Gemella sanguinis (species-level) has been reported as enriched in obesity cohorts [25, 26]; and Streptococcus parasanguinis (species-level) has been associated with hepatic steatosis, visceral-fat remodelling and impaired glucose regulation [27, 28]; Porphyromonas endodontalis (species-level) has been reported as enriched in periodontitis and obesity cohorts [29].

Finally, 6 strains exhibited mixed profiles. GGB7107 (SGB10420) improved CGM stability but increased liver inflammation and fibrosis. Fusobacterium nucleatum (SGB6001) also lowered CGM variability while related to higher adiposity and lower lean mass; this is consistent with Fusobacterium nucleatum (species-level) being linked to systemic metabolic disruption [30]. Porphyromonas pasteri (SGB2043) improved liver inflammation/fibrosis and reduced CGM variability, but was associated with higher body fat and lower lean mass; this aligns with Porphyromonas pasteri (species-level) reports of increased liver inflammation/steatosis and higher body fat despite effects on glycemic regulation [31, 32]. Trueperella pyogenes (SGB17137) showed a similar split: beneficial to the liver health and lower CGM variability, but higher glucose and higher body fat. Alloprevotella rava (SGB1485) and Alloprevotella tannerae (SGB1411) reduced liver inflammation and fibrosis, but were associated with increased body / visceral adiposity and lower lean mass. These directions are consistent with Alloprevotella rava (species-level) and Alloprevotella tannerae (species-level) reports on inflammatory modulation alongside adiposity/liver changes [33–35]. To our knowledge, GGB7107 (SGB10420) and Trueperella pyogenes (SGB17137) had no associated reports related to metabolic health.

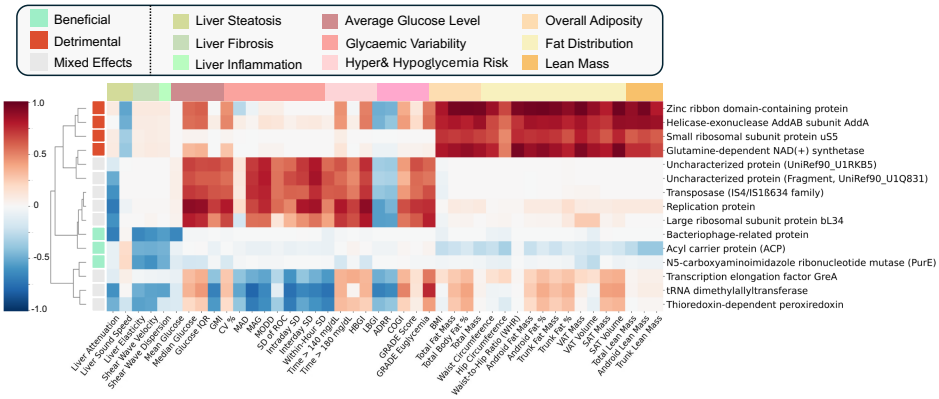

Fig. 3: Heatmap illustrating the associations between 15 core oral microbial gene families and 44 metabolic phenotypes. The selection method is detailed in Methods 4.6.

2.3.2 Significant gene families

We identified gene families positively associated with metabolic health, primarily in core biosynthetic functions. For example, Acyl carrier protein (ACP; D4FQK5) associated with lower hepatic fat/inflammation and reduced visceral adiposity and body weight. Mechanistically, ACP serves as a core scaffold protein in the fatty acid biosynthesis pathway, and enhanced fatty acid metabolism can alleviate liver steatosis and inflammation [36]. In addition, we also observed beneficial associations for uncharacterised genes, Bacteriophage-related protein (E7RXK3) from Lautropia mirabilis and N5-carboxyaminoimidazole ribonucleotide mutase (E6IZN5) from Streptococcus spp were both associated with improved liver health and glycemic indicators, to our knowledge, neither gene nor its source taxon has been linked to metabolic regulation.

A subset of gene families showed consistent adverse associations with metabolic health, mainly involved in translation, microbial proliferation, stress responses, and central metabolic regulation. Two ribosomal protein genes, the helicase-exonuclease AddAB subunit AddA (E4LF01) and the small ribosomal subunit protein uS5 (E6KU65), were associated with poorer liver function, increased adiposity, and increased body weight. The liver-related associations are supported by previous studies showing that ribosomal proteins are upregulated during dysbiosis and inflammation [37], and that increased ribosome biogenesis can directly promote hepatocyte proliferation and hepatic lipid accumulation [38, 39]. However, their associations with increased total adiposity and body weight are novel, with no prior evidence reported. Additional signals implicated regulators of metabolite levels and gene expression. Zinc-ribbon domain protein (D9RUZ0) showed adverse associations across liver, glycemic and adiposity traits; although direct evidence is lacking, its source genus Prevotella has been implicated in metabolic dysfunction [40–42]. Similarly, glutamine-dependent NAD^+ synthetase (E6KUD8) was associated with overall worsening, consistent with data that supra-physiologic NAD^+ promotes gluconeogenesis, impairs insulin signaling and enhances lipogenesis [43, 44].

We also observed mixed effects: signals that were beneficial for the liver but adverse for glycemic control. The unknown proteins U1RKB5 and U1Q831, IS4/IS1634 transposase (U1PZV2), a replication-associated protein (UPI0006850C96), and the large subunit ribosomal protein bL34 (U2QT17) were associated with lower liver fat, but higher glucose and greater glycemic variability. Genus-level context supports part of this pattern: U1RKB5 derives from Actinobaculum, which has been associated with improved liver and glycaemic profiles in NAFLD [45], and U1PZV2 from Actinomyces, enriched in MAFLD, encodes IS4/IS1634 transposases that may mobilize metabolic or drug-modifying genes, a potential route to glycemic effects [18, 46]; bL34 has also been implicated in metabolic syndrome and glucose dysregulation [47]. By contrast, U1Q831 and UPI0006850C96 currently lack functional or taxonomic links to host metabolism and merit follow-up. A second subset— Transcription elongation factor GreA (Z4WWF6), peroxiredoxin (J4VRI0) and tRNA-modification enzyme (J6H4J2), which combined lower liver fat/inflammation with higher glucose but lower variability, consistent with the impact of tRNA-modification pathways on glucose control [48, 49].

2.3.3 Significant pathways

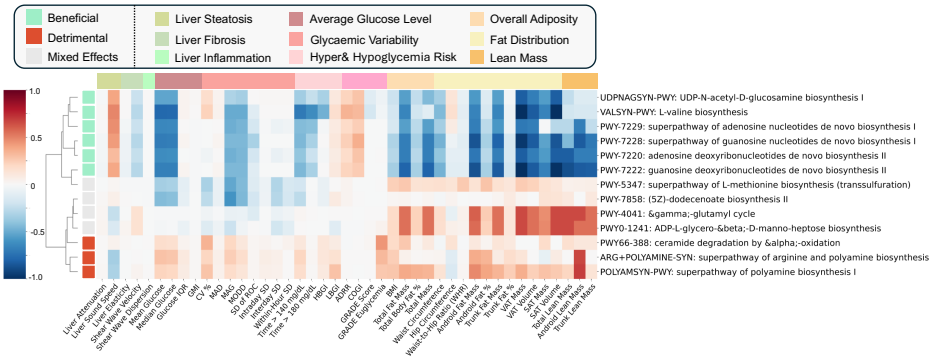

Fig. 4: Heatmap illustrating the associations between 13 core oral microbial pathways and 44 metabolic phenotypes. The selection method is detailed in Methods 4.6.

We highlight 6 pathways associated with beneficial metabolic profiles, particularly those involved in biosynthesis and energy metabolism. For example, UDP-N-acetyl-D-glucosamine biosynthesis (UDPNAGSYN-PWY) associated with better liver indices, more stable CGM and lower adiposity; non-oral evidence is directionally consistent for UDP-GlcNAc/hexosamine signalling [50]. L-valine biosynthesis (VALSYN-PWY) showed similar associations, aligning with BCAA supplementation benefits for glycemic control and hepatic lipid burden [51]. Additionally, Nucleotide de novo synthesis (tied to ATP/GTP) was broadly beneficial: purine routes (PWY-7229/-7220/-7222/-7228) correlated with better liver health, improved glycemic control and lower adiposity. Non-oral studies show these capacities decrease in obesogenic/diabetic states and increase with healthy exposures [52–54]; mechanistically, higher β-cell ATP/ADP promotes insulin secretion and lowers glucose [55].

In contrast, three pathways were detrimental to metabolic health: superpathway of arginine and polyamine biosynthesis (ARG+POLYAMINE-SYN) and superpathway of

polyamine biosynthesis I (POLYAMSYN-PWY) showed negative associations: higher pathway abundance correlated with worse liver indices (lower liver sound speed and greater inflammation–fibrosis), higher glucose and CGM variability, and higher body weight/adiposity. Non-oral evidence is directionally consistent—polyamine excess is linked to obesity, inflammation, and impaired insulin signaling, and oral multi-omics work reports elevated oral polyamines in obesity [56, 57]. Ceramide degradation by α-oxidation (PWY-66-388) was positively associated with glycemic deterioration—higher pathway abundance coincided with higher mean glucose and greater CGM variability. This direction is consistent with host evidence: higher ceramide species (core sphingolipids generated in host tissues) are linked to lipotoxicity, insulin resistance, and adverse metabolic outcomes [58, 59].

Mixed-direction pathways correlating with worse liver health but better glycemia and adiposity. These included the γ-glutamyl cycle (PWY-4041), ADP-L-glycero-β-D-manno-heptose biosynthesis (PWY-0-1241) and the L-methionine superpathway (PWY-5347). These patterns align with host biology: GSH sufficiency improves insulin sensitivity whereas hepatic oxidative stress worsens [60, 61]; mechanistically, ADP-heptose activates ALPK1–NF-κB [62], fitting the liver signal, although prior work reported higher glucose (opposite to our glycemic direction) and there is no evidence linking PWY-0-1241 to body composition. A sulphur-pathway duality (homocysteine vs cystathionine) may underlie PWY-5347 [63]. No prior evidence links (5Z)-dodecenoate biosynthesis II (PWY-7858) to metabolic health.

2.4 Community-level contribution to bacterial pathways

To better understand how bacterial communities contribute to functional pathways, we consider two possible modes: (1) a single bacterial taxon encodes the function; (2) multiple taxa collectively contribute to the pathway at the community level. To evaluate these possibilities in pathways associated with metabolic health, we analyzed functional profile data from the HPP dataset. This dataset quantifies contributions of specific genera and species to each pathway, based on their relative abundances.

Among the 299 pathways significantly associated with metabolic health, 9 (3.01%) involve only unclassified bacteria, while the remaining 290 (96.99%) are attributable to known bacterial genera and species. The number of contributing taxa varies across pathways, with an average of 72.20 ± 74.88 species and 26.45 ± 23.82 genera per pathway. Most pathways (275; 91.97%) involve more than one genus, (281; 93.98%) involve more than one species, suggesting that community-level interactions are common.

We further examined the taxonomic composition underlying the 14 most significant microbial pathways (Fig. 5). Beneficial pathways exhibited extensive taxonomic contributions, with 55–81 genera and 152–269 species involved per pathway (mean $= 66.33 \pm 9.33$ genera; 211.83 ± 37.85 species). In contrast, detrimental pathways involved a much narrower set of taxa, with only 3–7 genera and 4–18 species contributing per pathway (mean $= 5.33 \pm 2.08$ genera; 13.00 ± 7.81 species), suggesting more limited microbial involvement. Pathways showing mixed associations displayed intermediate complexity, with 18–35 genera and 35–72 species per pathway (mean $= 25.50 \pm 7.94$ genera; 57.25 ± 17.35 species).

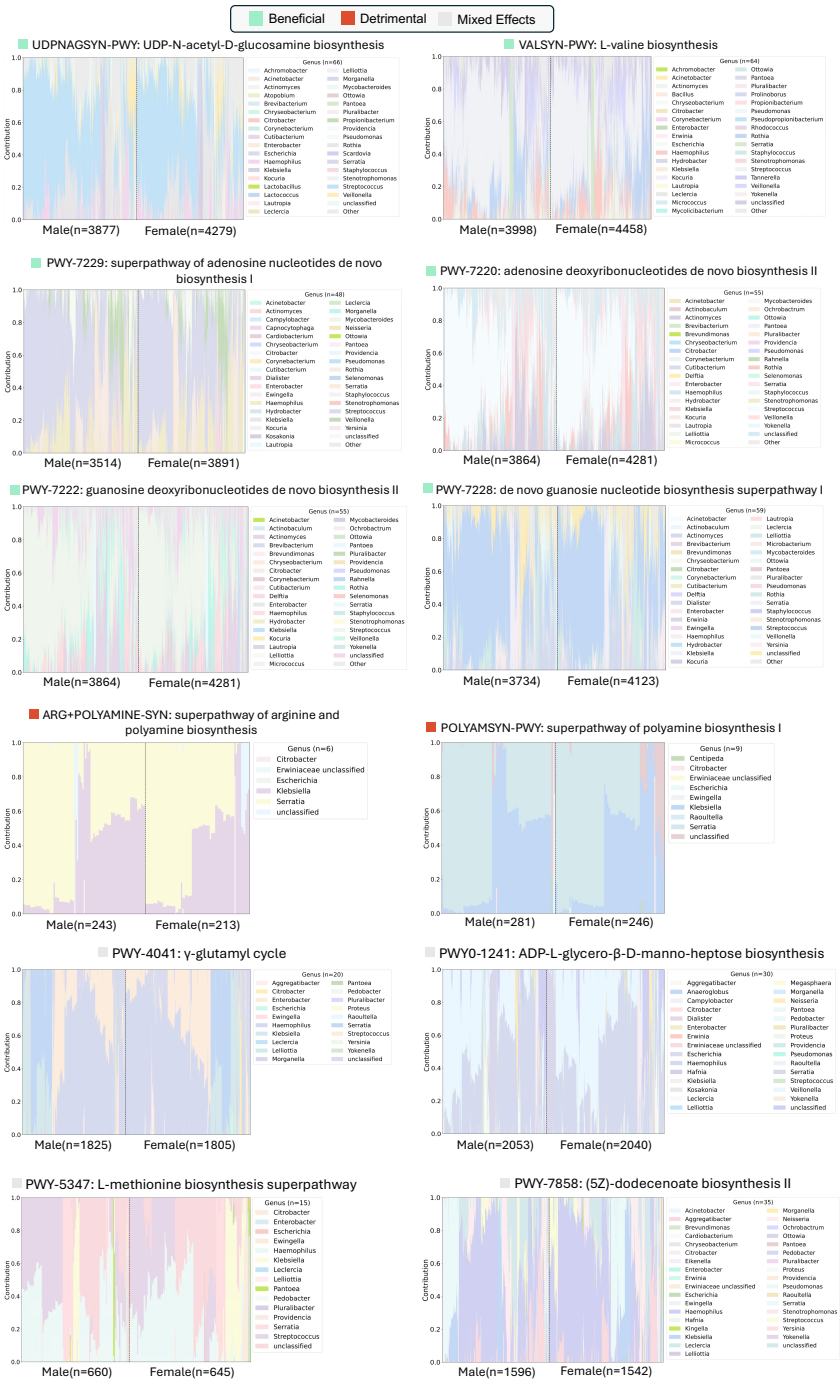

Fig. 5: Genus-level contributions to 12 selected pathways. Stacked areas show the proportional contribution of genera (y-axis) across male and female participants. Contributions derive from HUMAnN stratified profiles aggregated to the genus level. PWY-66-388 (ceramide degradation by α-oxidation) is not shown because it is dominated by Pseudomonas.

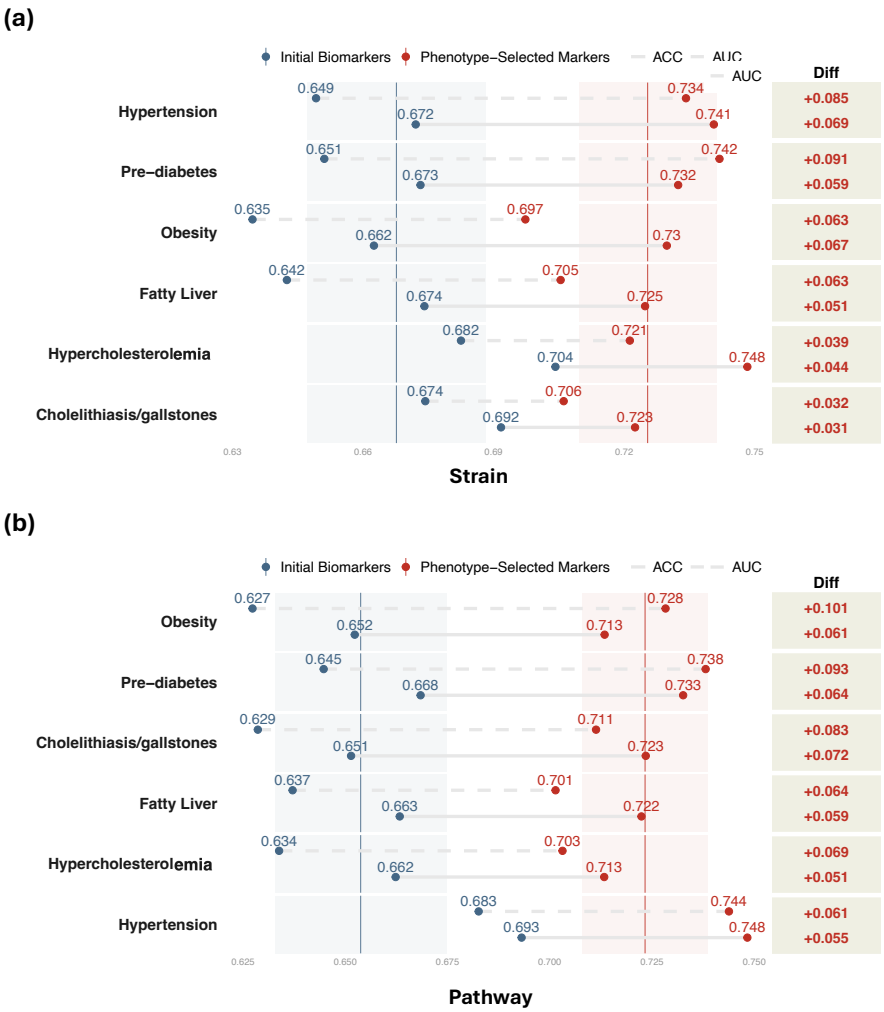

Fig. 6: Metabolic disease prediction performance using oral microbiome features at two resolutions. (a) Strain level; (b) Pathway level. For each condition, a baseline model using all initial features (blue) is compared with an optimized model restricted to phenotype-selected markers (red), the selection strategy is detailed in Methods 4.8 . The right-hand Diff column reports the absolute improvement of the optimized model over the baseline for AUC and accuracy (ACC).

These findings indicate that key microbial functions relevant to host metabolism are generally shaped through community-level encoding rather than driven by individual taxa. Despite variability in taxonomic resolution, beneficial pathways consistently involved a higher number of unclassified microbial contributors (mean $= 3.43 \pm 1.51$, range: 2–6), compared to those in detrimental (1.67 ± 0.58, range: 1–2) and mixed

pathways (1.50 ± 0.58, range: 1–2). While the presence of unclassified contributors introduces minor uncertainty, their limited number suggests a negligible impact on the robustness of these community-level patterns.

2.5 Metabolic diseases prediction

To evaluate the potential of the oral microbiome as a non-invasive diagnostic tool for metabolic diseases, we constructed machine learning models to distinguish between healthy and diseased states across six common metabolic conditions: hypertension, obesity, pre-diabetes, fatty liver, hypercholesterolemia, and cholelithiasis/gallstones. To assess biological relevance while preventing information leakage, we compared two model frameworks: (1) a full model incorporating all discovery-stage microbial markers, and (2) a phenotype-filtered model, in which feature selection was restricted to training folds and limited to markers associated with pre-specified clinical phenotypes not used to define case status for the target disease (see Methods 4.8 for selection criteria and leakage controls).

Biologically informed feature selection consistently and significantly improved predictive performance across all six diseases (Fig. 6). For example, in hypertension prediction using strain-level features, the phenotype-filtered model increased the AUC from 0.649 to 0.734 (+0.085) and accuracy from 0.672 to 0.741 (+0.069). Similar performance gains were observed at the pathway level; for example, in prediction of Obesity, the AUC improved from 0.627 to 0.728 (+0.101), and Accuracy improved from 0.652 to 0.713 (+0.061).

To further elucidate the biological signals driving disease prediction, we conducted feature importance analyses on the optimized models. Several beneficial and detrimental markers previously characterized in Results 2.2 and 2.3 consistently ranked among the most predictive features. In particular, for fatty liver and pre-diabetes, Porphyromonas taxa and the polyamine biosynthesis pathway emerged as high-impact predictors, whereas the beneficial strain Corynebacterium durum was strongly associated with healthy status. Overall, results highlight the diagnostic potential of oral microbial features and provide independent predictive validation of the biological associations identified earlier. In addition, microbial signatures linked to host metabolic phenotypes not only correlate with, but also effectively discriminate metabolic disease states, reinforcing their relevance as potential biomarkers.

2.6 Validation in an independent cohort

To ensure the reproducibility and generalizability of our findings, we conducted a validation analysis in an independent large-scale cohort comprising 20,293 individuals. This cohort included oral metagenomic profiles paired with matched phenotypic data (n = 10,081 males, 10,212 females; age range: 1–80 years; mean $\pm$ SD: 32.02 $\pm$ 24.75 years; BMI: 25.64 $\pm$ 7.73 kg/m^2; waist circumference: 87.10 $\pm$ 22.31 cm). To ensure methodological comparability, metagenomic processing, phenotype definitions, and association modeling were performed identically to those applied in the HPP discovery cohort (Methods 4.9).

We assessed the robustness of strain-level associations to validate the reproducibility of key microbial–host relationships in an independent cohort. Because strain-level resolution was not available in the replication dataset, the 96 BMI-associated strains were collapsed to 38 non-redundant genera via a many-to-one mapping procedure (Methods 4.9). Among these 38 genera, 17 (44.7%) exhibited significant associations in the same direction, and 14 of these (82.4%) demonstrated concordant effect estimates. Similarly, of the 98 strains associated with waist circumference, 41 corresponding genera were evaluated; 16 (39.0%) were replicated, and 14 (87.5%) displayed consistent effect directions. To complement the strain-derived validation, we performed a parallel genus-level replication analysis. Among the 29 BMI-associated genera in the discovery cohort, 14 (48.3%) were also significantly associated in the replication cohort, with 12 (85.7%) showing directional concordance. For waist circumference, 11 of the 30 associated genera (36.7%) were replicated, 10 (90.9%) of which exhibited consistent directions of effect.

In conclusion, these multi-level replication analyses demonstrate partial but directionally consistent reproducibility under genus-level resolution, thereby supporting the robustness and external validity of the key oral microbial associations identified in the HPP cohort.

3 Discussion

In recent years, the oral microbiome has been consistently linked to host metabolic health, with associations reported for obesity, type 2 diabetes, and non-alcoholic fatty liver disease (NAFLD) [8, 9]. Therapeutic approaches targeting the oral ecosystem, such as periodontal treatment, oral probiotics, and microbiota modulators, have shown potential to improve liver function, glycemic control, and body fat composition, and are increasingly regarded as adjunctive treatments for metabolic disorders [64–66].

Despite recent advances, systematic, population-scale evidence linking the oral microbiome at strain-level and functional (gene family and pathway) resolution to metabolic health remains limited. To address this gap, we analyzed 9,431 participants in the Human Phenotype Project and linked oral metagenomes to 44 phenotypes across liver ultrasonography, CGM, and body composition. We constructed a three-layer map across strains, gene families, and pathways and linked oral metagenomes to 44 phenotypes. We identified 213 strains, 124,603 gene families, and 299 pathways that were associated with at least one phenotype. Associations were pleiotropic yet system-specific: most features spanned multiple phenotypes, but about half were confined to a single system. Strain signals concentrated in body composition, with strong positive links to adiposity and weaker links to lean mass. In the functional layer, CGM contributed most associations and system-specific signals, with positive directions for mean glucose and hyperglycemia risk and negative directions for hypoglycemia risk and glycemic variability. The liver domain showed the fewest associations and the directions of the strains and pathways differed between inflammation and fibrosis.

Next, we prioritized features with the broadest and most robust relationships to metabolic health. Where strain-level reports were unavailable in the literature, we contextualized findings at the species or genus level and, when oral precedents were

limited, with non-oral evidence anchored by relevant metabolites and pathway products. With few exceptions, directions were concordant with prior reports. At the strain layer, beneficial strain profiles aligned with oxygen tolerance or nitrate use and with lower liver inflammation and fibrosis. Detrimental profiles were enriched for anaerobic, inflammophilic fermenters associated with higher glucose, steatosis, and visceral adiposity. Mixed profiles showed system-dependent trade-offs. At the gene-family layer, beneficial signals clustered in core biosynthesis, while detrimental signals concentrated in translation and replication modules and in glutamine-dependent NAD^+ synthetase. These patterns point to partial uncoupling between liver status and glucose control. At the pathway layer, UDP-N-acetylglucosamine and UDP-N-acetylgalactosamine biosynthesis, L-valine biosynthesis, and de novo purine biosynthesis aligned with healthier liver indices, more stable CGM profiles, and favorable fat distribution. In contrast, polyamine biosynthesis and ceramide alpha-oxidation aligned with adverse outcomes. Contributions to these pathways typically arose from multiple genera or species rather than a single taxon, consistent with community-level functionality.

We also trained prediction models using oral features that were significantly associated with metabolic phenotypes. Models built from selected features outperformed full feature models on several conditions (detail result shown in Results 2.2), indicating stronger and more coherent links to disease risk.

This study advances understanding of oral–metabolic links but has limitations. First, participants were recruited from a single geography in Israel, which may limit generalizability, and replication was feasible only at the genus level because strain-level data were unavailable in the external cohort, leading to weaker effects than at the strain level despite careful matching. Second, functional inference relies on metagenomic annotation and reference databases; low abundance, rare, or poorly characterized taxa and gene families may be underestimated.

Despite these limitations, high-resolution strain and functional evidence remains limited in the field, and our cohort-scale map directly addresses this gap. The sample size and breadth of phenotyping provide robustness and potential transportability relative to small cohorts, and the prioritized features supply reusable candidates for future work. From an applied perspective, oral markers merit evaluation as noninvasive tools for metabolic risk stratification and early screening. On the other hand, reinforcing beneficial community functions and selectively suppressing detrimental pathways could guide the development of microbiome-based therapeutics for metabolic disease.

4 Methods

4.1 Description of HPP cohort

The Human Phenotype Project (HPP) is a large-scale, longitudinal deep-phenotyping cohort of 9,431 individuals aged from 38 to 72. Since January 2019, the HPP has concurrently collected a wide range of multimodal data covering multiple major physiological systems. These data modalities include: tabular data recording personal medical history and physiological information; deep molecular data encompassing genomics, proteomics, and microbiomics; time-series data reflecting dynamic physiological changes, such as continuous glucose monitoring; and key imaging data,

including liver ultrasound and DXA scans. Data is available at the HPP data website, and HPP study was conducted according to the principles of the Declaration of Helsinki and approved by the Institutional Review Board (IRB) of the Weizmann Institute of Science (reference no. 1719-1).

In this study, we used metagenomic data from oral swabs in the HPP cohort and combined these with three core metabolic assessments: (1) liver health status, obtained by liver ultrasonography; (2) dynamic glucose homeostasis, acquired through CGM; and (3) body composition, including visceral adipose tissue, as measured by DXA. These data provide a basis for analyzing the potential relationships between the oral microbiome and metabolic phenotypes.

4.2 Oral Microbiome Collection and Preprocessing

Oral microbiome samples were collected via buccal swabs during the baseline visit and processed at Gencove laboratories for DNA extraction and library preparation. Subsequent low-pass whole genome sequencing was performed at Neogen GeneSeek Laboratories on an Illumina NovaSeq platform, utilizing a 150-bp paired-end read configuration.

Raw sequencing reads were first aligned to the human reference genome to isolate non-human reads. These reads were then subjected to quality control using Trimmomatic to remove sequencing adapters and low-quality sequences. The quality-controlled reads were then processed through a dual analysis pipeline. The taxonomic composition was profiled with MetaPhlAn 4 to determine the relative abundance of microbial taxa from kingdom to strain level. Concurrently, functional potential was characterized with HUMAnN 3.6 to quantify the abundance of microbial gene families and metabolic pathways. The resulting taxonomic and functional profiles, derived from the processed non-aligned (non-human) reads, were preprocessed for microbiome analyzes.

After host-depletion and read-level QC, we retained features (strains, gene families, pathways) with ≥ 200 non-zero observations across samples. For each retained feature, we defined a feature-specific detection threshold as the 1st percentile of its positive abundances and replaced zero entries with half of this threshold to avoid large pseudocount bias.

Let $\tilde{A}_{if} \geq 0$ denote the resulting (zero-replaced) abundance of feature f in sample i, and let $\mathcal{F}$ be the feature set. We then performed within-sample total-sum normalization and scaling. To stabilize variance and improve approximate normality in downstream association models, we subsequently applied a base-10 log transformation. These steps are defined as follows:

$$
\begin{aligned}
T_i &= \sum_{f \in \mathcal{F}} \tilde{A}_{if}, \\
R_{if} &= \frac{\tilde{A}_{if}}{T_i}, \\
\mathrm{PPM}_{if} &= 10^6 \times R_{if}, \\
Y_{if} &= \log_{10}\big(\mathrm{PPM}_{if}\big).
\end{aligned}
$$

Because of zero replacement, $\mathrm{PPM}_{if} > 0$ and the logarithm is well-defined. All steps were applied identically to strains, gene families and pathways.

We further filtered the taxonomic attributions for each pathway provided by HUMAnN. To reduce noise from low-prevalence organisms, only genera and species that contributed to a pathway's abundance in at least 200 samples were retained for subsequent analysis.

4.3 Metabolic health phenotypes collection and preprocessing

In this study, we selected phenotypes related to liver health, glucose homeostasis, and body composition, as these are well-established and critical indicators of metabolic health. The detailed descriptions are listed as follows:

Liver: Participant liver health is quantitatively assessed using a Supersonic Aixplorer MACH 30 ultrasound system (Hologic, USA) with a C6-1X convex transducer. Following a standardized protocol, measurements are taken from three distinct locations within the right liver lobe via an intercostal approach while participants are supine and holding their breath. To ensure measurement quality for elasticity and viscosity, a stability index greater than 90% was required. This procedure yields key quantitative metrics for assessing fibrosis (Elasticity), inflammation (Viscosity), and steatosis (Sound Speed and Attenuation), providing a final dataset with values in units such as kPa and Pa·s.

CGM: Dynamic glucose homeostasis is assessed using the FreeStyle Libre ProIQ Flash continuous glucose monitoring (CGM) device. During the baseline visit, a sensor is placed on the back of the participant's upper arm and activated for a two-week period, recording interstitial glucose levels every 15 minutes. Concurrently, participants log information on their medication, physical activity, and sleep hours using a dedicated application (10K application). This method yields a high-resolution time-series of glucose levels, from which various summary metrics of glycemic control and variability (e.g., mean glucose, coefficient of variation, time in range) are calculated using the iglu R package [67].

Body Composition: Body composition and bone mineral density are assessed by Dual-energy X-ray Absorptiometry (DXA) using a GE Lunar Prodigy Advance device (GE Healthcare, USA). For the total body scan, participants are positioned supine after removing all metal items and heavy clothing. This scan provides detailed measurements of fat mass, lean mass, and percent body fat for the whole body and for specific regions (arms, legs, trunk, android, and gynoid). Furthermore, the GE CoreScan software is used to quantify Visceral Adipose Tissue (VAT) and Subcutaneous Adipose Tissue (SAT) within the android region, while bone mineral density is specifically measured at the bilateral femur necks and the L1-L4 lumbar spine.

For each phenotype p from the liver, CGM, and body composition systems, we performed the data cleaning process. To obtain robust location and scale, we computed the shortest interval covering 95% of the non-missing observations and estimated the mean μ_p and standard deviation σ_p within that interval. We then removed extreme outliers defined by the condition $|x_{ip} - \mu_p| > 8\sigma_p$. For the remaining values, we applied

winsorization at $\pm 5\sigma_p$:

$$x_{ip}^{\text{win}} \;=\; \min\Big(\max\big(x_{ip},\, \mu_p - 5\sigma_p\big),\, \mu_p + 5\sigma_p\Big).$$

These cleaned phenotypes were used in all downstream microbiome–phenotype association analyses.

4.4 Identification of significant strain, gene family, pathway association

Associations between oral strain, gene family, and pathway profiles and 44 host metabolic phenotypes were assessed using ordinary least squares (OLS) linear regression models. These models were implemented with the statsmodels package (v0.14.4) in Python (v3.11), with adjustments for age, sex, and smoking status. The analysis environment was Ubuntu 22.04, utilizing the numPy (v1.26) and pandas (v2.2) libraries. The microbial features were first preprocessed using Methods 4.2, while phenotypic variables were cleaned using Methods 4.3. For each association, we estimated effect coefficient and corresponding P-values. Bonferroni correction was performed independently for each of the three microbial feature types: strains, gene families, and pathways. Within a type, the P values were adjusted for the entire set of feature-phenotype tests across all phenotypes. An association with a Bonferroni-adjusted P-value < 0.05 was considered statistically significant.

4.5 Mining for core gene family

Given the large number of gene families identified (N = 355,674), we anticipated significant challenges from high inter-correlation and functional redundancy. To address this, we designed and implemented two orthogonal approaches: a pre-association decorrelation filter and a post-association independence pruning step. The pre-association filter was applied prior to association testing to generate a reduced set of representative, uncorrelated gene families. In contrast, the post-association pruning was applied after the main analysis to distill the list of significant associations down to a set of statistically independent signals for each phenotype.

Pre-association decorrelation filter: To mitigate collinearity among bacterial gene families prior to association testing, we applied a pre-association decorrelation filter. All gene families were randomly partitioned into batches of up to 3,000 features. Within each batch, we computed pairwise Spearman rank correlations and applied average-linkage hierarchical clustering using a correlation cutoff of 0.3 to define clusters. For each cluster, we generated a candidate subset by ranking features according to their mean abundance across samples and retaining the top 5%. Pairwise proximity among candidates was quantified as

$$d_{ij} = 1 - |\rho_{ij}|,$$

and the cluster representative was defined as the feature with the smallest mean distance to all other candidates.

After identifying representative gene families from each batch, we pooled these features and reapplied the clustering procedure iteratively for three successive rounds to further suppress inter-feature redundancy. This iterative decorrelation process produced a final feature set with minimal mutual correlation. The resulting retained gene families exhibited an average pairwise correlation of 0.01 (mean absolute Spearman's ρ, $P < 1 \times 10^{-3}$) with an overall standard deviation of 0.26, indicating substantial independence among the selected features.

Post-association pruning: After identifying gene families associated with metabolic health, we applied a pruning strategy to determine a subset of gene families exhibiting independent associations with the relevant host metabolic phenotypes. After the association analysis (Methods 4.4), for each metabolic phenotype Y_k we retained gene families g with Bonferroni-adjusted p-values $p_{g,k}^{\text{adj}} < 0.05$ and their regression coefficients $\hat{\beta}_{g,k}$, where X_g denotes the abundance of gene family g. To place coefficients on a phenotype-specific, unit-free scale, we computed the standardized effect size

$$S_{g,k} = |\hat{\beta}_{g,k}| \cdot \frac{\text{SD}(X_g)}{\text{SD}(Y_k)}.$$

Within phenotype k, candidates were ranked by a joint rank that treats significance and effect size symmetrically:

$$R_{g,k} = \text{rank}(p_{g,k}^{\text{adj}}) + \text{rank}(-S_{g,k}),$$

For each phenotype Y_k, we selected the top-ranked candidate (by $R_{g,k}$), and added it to the approximately independent set, and removed any remaining candidate whose Spearman correlation with the lead satisfied $\rho \geq 0.30$. We iterated until no candidates remained, yielding a set of independent gene families for each phenotype.

4.6 Identification of key oral microbial features associated with metabolic health

We developed a systematic selection strategy to identify the key oral microbial strains, gene families, and pathways most strongly and broadly associated with host metabolic phenotypes. To capture system-level diversity, all phenotypes were first organized into three metabolic domains: liver, continuous glucose monitoring (CGM), and body composition. Within each system, we quantified the association breadth of every microbial feature by counting the number of phenotypes with which it showed a significant relationship (Bonferroni-corrected $p < 0.05$). Strains and pathways were then ranked according to this association count, such that features linked to a larger number of phenotypes received higher priority. For gene families, we began with the post-association pruned set obtained after correlation-based clumping (Methods 4.5), ensuring that the candidate features were functionally independent and not phenotypically redundant. These pruned gene families were then ranked within each system using the same association-based metric. From each of the three systems, we selected the top five ranked features per data type (strain, gene family, and pathway) as the key microbial components for downstream analyses. In order to avoid the repeated representation of cross-system features, we performed de-duplication step by merging identical features

across systems into a unified, non-redundant set. This hierarchical selection procedure prioritized features that were not only statistically significant but also robustly associated across multiple related phenotypes, resulting concise and biologically meaningful set of core oral microbial markers.

4.7 Classification of oral microbial features

Each microbial feature (strain, gene family, or pathway) was classified as Beneficial, Detrimental, or Mixed by integrating its association directions across physiological systems (liver, CGM, and body composition), without cross-system averaging. Starting from Bonferroni-significant feature–phenotype associations, we oriented all phenotypes to a common health axis using a a pre-specified mapping: for phenotypes where higher values indicate better health, the original association sign was retained; for those where lower values indicate better health, the sign was inverted. The full phenotype-specific orientation scheme is provided in Supplementary Table S2. This approach to direction-of-effect synthesis, coupled with transparent reporting of grouping and weighting rules, follows established best practices for evidence synthesis without meta-analysis.

Within each system, phenotypes were grouped into pre-defined clinical domains, and all significant associations within a given system–domain combination were collapsed into a single domain-level vote using a weighted-majority scheme. This procedure preserved directional coherence while reducing redundancy among correlated phenotypes. Association-level weights preserved the dynamic range of evidence but capped extremes, $w = \min\{3, -\log_{10}(P_{\text{bonferroni}})\}$; domain weights were normalized so the sum per system equaled 1. For system s, we defined the weighted positive proportion below:

$$\text{WPP}_s = \sum_{d \in s} \tilde{W}_{s,d}\, \mathbf{1}(\hat{y}_{s,d} = +1)\,, \qquad \begin{cases} \text{Beneficial}, & \text{WPP}_s \geq 0.90, \\ \text{Detrimental}, & \text{WPP}_s \leq 0.10, \\ \text{Mixed}, & \text{otherwise.} \end{cases} \tag{1}$$

where $\hat{y}_{s,d}$ denotes the domain-level vote and $\tilde{W}_{s,d}$ the normalized domain weight. These classifications follow the same three-system framework and domain definitions (described in the main text).

4.8 Metabolic diseases prediction

We modeled each condition independently in the HPP cohort using balanced case–control data. Case counts were: Hypercholesterolemia ($n = 2409$), hypertension ($n = 695$), pre-diabetes ($n = 449$), obesity ($n = 589$), fatty liver ($n = 623$), and cholelithiasis/gallstones ($n = 650$). For each disease, an equal number of controls was randomly sampled from the HPP healthy pool; sampling was performed separately for each disease among participants carrying an explicit healthy label. Models were fit at two feature layers—strain and pathway—from the corresponding oral microbiome abundance profiles. The baseline classifier was LightGBM, evaluated with five-fold cross-validation on the balanced sets.

To test a biologically informed, lower-dimensional alternative, we implemented a phenotype-filtered variant. Within each training fold for the target disease, we ranked pre-specified clinical phenotypes (none used to define case status) by the strength and significance of their association with the disease; we retained the Top-20 phenotypes and, using Results 4.4 restricted to the same training data, selected oral markers (strains or pathways) that were Bonferroni-significant for any of these phenotypes. The classifier was then trained only on this training-defined marker set. For the held-out test fold, the fixed Top-20 list and marker set were applied unchanged to construct inputs, with no recomputation or reselection on test data—this safeguards against data leakage. For each disease and feature layer, performance was summarized across the same five cross-validation splits for both pipelines (full features vs. phenotype-filtered) to enable paired comparisons.

4.9 Replication study

We evaluated external reproducibility in an independent cohort from the U.S. National Health and Nutrition Examination Survey (NHANES) comprising 20,293 participants with oral microbiome profiles at the genus level and matched anthropometrics (females: $n = 10{,}212$; males: $n = 10{,}081$; age 32.02 ± 24.75 years; BMI 25.64 ± 7.73,kg/m^2; waist circumference 87.10 ± 22.31cm). To harmonize analyses with the discovery cohort, we applied the same preprocessing and association framework where applicable (details in Methods 4.2, 4.3, and 4.4).

Because the replication resource does not provide strain resolution or functional profiles, we assessed robustness of strain–phenotype signals at the genus level using two complementary strategies. Strategy 1 (strain→genus mapping): each discovery strain significantly associated with BMI or waist circumference was mapped to its corresponding genus (many–to–one). Replication was declared for a genus if it was significantly associated with the same phenotype in NHANES and the effect direction matched that observed in discovery. Strategy 2 (genus–level re-analysis in discovery): to mitigate resolution mismatch, we recomputed genus–phenotype associations within the discovery cohort using the same models and thresholds, then tested whether the corresponding genera in NHANES showed significant effects in the same direction. Missing phenotypes or covariates were handled by listwise exclusion.

No replication was attempted for gene families or pathways because such functional abundances are unavailable in NHANES oral data.

5 HPP data availability:

Owing to privacy and ethical considerations set forth by the IRB committee of the study, all datasets that are part of the Human Phenotype Project (HPP)—such as blood test results and anthropometrics measurements—are accessible to researchers at universities and other research institutions at: HPP Data Access Portal. Interested bona fide researchers should contact info@pheno.ai, who will then provide an agreement that allows access to the data for non-commercial purposes. Data access will then be provided through an account in a secure cloud-based environment.

6 Code availability:

Code used in this study is available at the following GitHub link: https://github.com/haochen-MBZUAI/HPP-Oral-Microbiome.

Table S1: Statistic of Liver, CGM, and Body Composition Phenotypes

Phenotype	Male n=4474(47.4%)	Female n=4957(52.6%)	All n=9431
Liver Health			
Liver Steatosis			
Liver sound speed (m/s)	1547.36 (23.07)	1539.51 (23.69)	1543.31 (23.72)
Liver attenuation (dB/cm/MHz)	0.41 (0.10)	0.41 (0.10)	0.41 (0.10)
Fibrosis			
Liver Elasticity (kPa)	5.43 (1.25)	4.68 (0.94)	5.04 (1.17)
Shear Wave Velocity (m/s)	1.34 (0.14)	1.24 (0.12)	1.29 (0.14)
Inflammation			
Liver Viscosity (Pa·s)	1.70 (0.24)	1.62 (0.27)	1.66 (0.26)
Shear Wave Dispersion ((m/s)/kHz)	2.46 (0.45)	2.32 (0.50)	2.39 (0.48)
Glycemic Control (CGM)			
Average Glucose Level			
Mean Glucose (mg/dL)	97.35 (13.74)	94.08 (11.23)	95.63 (12.59)
Median Glucose (mg/dL)	94.31 (11.72)	91.30 (10.67)	92.73 (11.28)
Glucose Management Indicator (GMI, %)	5.64 (0.33)	5.56 (0.27)	5.60 (0.30)
Glycemic Variability			
Glucose IQR (mg/dL)	17.98 (6.78)	17.02 (4.98)	17.48 (5.92)
Coefficient of Variation (CV, %)	15.95 (4.18)	16.15 (4.00)	16.05 (4.09)
Mean Absolute Deviation (MAD, mg/dL)	12.62 (4.69)	11.91 (3.38)	12.25 (4.05)
Mean of Daily Differences (MODD, mg/dL)	13.62 (4.93)	12.88 (4.04)	13.23 (4.50)
Mean Absolute Glucose (MAG)	10.85 (2.94)	10.64 (2.73)	10.74 (2.83)
SD of ROC	0.4430 (0.1002)	0.4352 (0.0944)	0.4389 (0.0973)
SD between Time Points (Time-of-Day SD)	7.73 (2.98)	7.97 (2.82)	7.86 (2.91)
SD between Days (Interday SD)	13.81 (3.76)	13.70 (3.53)	13.75 (3.64)
Within-Hour SD	5.29 (1.24)	5.18 (1.16)	5.23 (1.20)
Hyper/Hypoglycemia Risk			
High Blood Glucose Index (HBGI)	0.23 (0.94)	0.14 (0.36)	0.18 (0.70)
Low Blood Glucose Index (LBGI)	2.18 (1.91)	2.57 (1.94)	2.39 (1.93)
Time > 140 mg/dL (%)	2.44 (3.15)	2.05 (2.83)	2.23 (3.00)
Time > 180 mg/dL (%)	0.08 (0.19)	0.07 (0.18)	0.07 (0.19)
Average Daily Risk Range (ADRR)	10.32 (4.70)	11.27 (4.78)	10.82 (4.77)
Glycemic Control Quality			
Composite Glycemic Index (COGI)	0.89 (0.16)	0.86 (0.17)	0.87 (0.16)
Diabetes Risk Assessment (GRADE)	1.37 (1.23)	1.24 (0.85)	1.30 (1.05)
GRADE Euglycemia	68.08 (21.92)	65.30 (21.69)	66.62 (21.84)
Body Composition			
Overall Adiposity			
BMI (kg/m^2)	26.70 (3.77)	25.75 (4.40)	26.21 (4.13)
Total Fat Mass (kg)	23.16 (8.05)	25.98 (8.56)	24.60 (8.43)
Total Body Fat (%)	28.52 (6.32)	38.71 (6.79)	33.71 (8.31)
Total Mass (kg)	79.48 (12.53)	65.66 (11.89)	72.44 (14.03)
Fat Distribution			
Waist Circumference (cm)	94.62 (10.87)	84.07 (10.99)	89.24 (12.14)
Hip Circumference (cm)	102.43 (7.43)	102.57 (9.37)	102.51 (8.48)
Waist-to-Hip Ratio (WHR)	0.92 (0.07)	0.82 (0.07)	0.87 (0.09)
Android Fat Mass (g)	2327.65 (1105.68)	2071.05 (963.79)	2196.94 (1043.69)
Android Fat %	0.35 (0.10)	0.40 (0.10)	0.37 (0.10)
VAT Mass (g)	1211.70 (748.66)	647.77 (458.77)	924.62 (679.53)
VAT Volume (cm^3)	1279.13 (776.47)	686.63 (486.30)	977.44 (709.95)
Trunk Fat Mass (g)	13370.60 (5358.01)	12929.46 (5013.76)	13145.68 (5189.87)
Trunk Fat %	0.32 (0.08)	0.38 (0.09)	0.35 (0.09)
SAT Mass (g)	1397.79 (683.01)	1600.33 (749.12)	1500.89 (724.50)
SAT Volume (cm^3)	1481.66 (723.99)	1696.35 (794.07)	1590.95 (767.97)
Lean Mass			
Total Lean Mass (kg)	56.33 (6.82)	39.67 (4.98)	47.84 (10.23)
Android Lean Mass (kg)	4.07 (0.57)	2.90 (0.43)	3.48 (0.77)
Trunk Lean Mass (kg)	27.10 (3.31)	19.63 (2.48)	23.29 (4.74)

Table S2: Description of All Metabolic Health Phenotypes

Phenotype	Short Description	Impact
Liver Health		
Liver Sound Speed	Sound Speed Plane-Wave Ultrasound.	Beneficial
Liver Attenuation	Attenuation Plane-Wave Ultrasound coefficient, measuring the decrease in amplitude of the ultrasound waves as a function of frequency.	Harmful
Liver Elasticity	Elasticity, median of the values measured within the Q-Box.	Harmful
Shear Wave Velocity	Velocity of the shear wave, median of the values measured within the Q-Box.	Harmful
Liver Viscosity	Viscosity, median of the values measured within the Q-Box.	Harmful
Shear Wave Dispersion	Shear wave dispersion median of the values measured within the Q-Box.	Harmful
Glycemic Control (CGM)		
Mean Glucose	Mean of all glucose values.	Harmful
Median Glucose	Median of all glucose values.	Harmful
GMI	A linear transformation of the mean glucose value, meant to improve the eA1C measure.	Harmful
Glucose IQR	Interquartile range (IQR), calculated as the distance between the 25th percentile and the 75th percentile of the glucose values.	Harmful
CV	Coefficient of variation of all glucose values.	Harmful
MAD	Median Absolute Deviation (MAD). This is a measure of glycemic variability, which is calculated by taking the median of the differences between glucose values and their median.	Harmful
MODD	Mean difference between glucose values obtained at the same time of day (MODD). This is a measure of glycemic variability that is calculated by taking the mean of the absolute differences between glucose values measured at the same time, a day apart.	Harmful
MAG	Mean Absolute Glucose (MAG). This is a measure of glycemic variability that's meant to be less dependent on the mean glucose value and to take into account all variability over time.	Harmful
SD of ROC	Standard deviation of all the rate of change (ROC) values of an individual. ROC is calculated between every two consecutive glucose measures.	Harmful
Time-of-Day SD	SD between time points. Standard deviation of the mean glucose value calculated for each time point across all days.	Harmful
Interday SD	Vertical SD within days. Average value of the SD values for each day separately.	Harmful
Within-Hour SD	SD within series. Taking hour-long intervals that start at each point of the glucose measures, the SD of each hour-long window is computed, and then the mean of all those SDs is taken.	Harmful
HBGI	High Blood Glucose Index (HBGI).	Harmful
LBGI	Low Blood Glucose Index (LBGI).	Harmful
Time > 140 mg/dL	Percent of glucose measures that were larger than 140 mg/dL.	Harmful
Time > 180 mg/dL	Percent of glucose measures that were larger than 180 mg/dL.	Harmful
ADRR	Average daily risk range (ADRR) is a variability measure that was designed to be sensitive to both hyperglycemia and hypoglycemia. The ADRR is composed of the HBGI and LBGI.	Harmful
COGI	Continuous Glucose Monitoring Index (COGI). COGI uses three measures of the CGM - time in range, time below range and glucose variability (GV) and averages them using a weighted mean, usually with weights of 50%, 35% and 15% accordingly.	Harmful
GRADE Score	Glycaemic Risk Assessment Diabetes Equation (GRADE). This clinical risk score aims to evaluate the degree of risk presented by a glucose profile.	Harmful
GRADE Euglycemia	Percentage of the GRADE score that is attributed to euglycemia (glucose values within the normal range, default is 70-140).	Beneficial
Body Composition		
BMI	Body Mass Index.	Harmful
Total Fat Mass	Body composition total body fat mass.	Harmful
Total Body Fat	Body composition total tissue percent fat.	Harmful
Total Mass	Body composition total tissue mass.	-
Waist Circumference	A measure of abdominal fat accumulation.	Harmful
Hip Circumference	A measure of hip width.	-
Waist-to-Hip Ratio	A key indicator of central obesity and metabolic risk.	Harmful
Android Fat Mass	Body composition android fat mass.	Harmful
Android Fat %	Body composition android tissue percent fat.	Harmful
VAT Mass	Total scan visceral adipose tissue (VAT) mass.	Harmful
VAT Volume	Total scan visceral adipose tissue (VAT) volume.	Harmful
Trunk Fat Mass	Body composition trunk fat mass.	Harmful
Trunk Fat %	Body composition trunk tissue percent fat.	Harmful
SAT Mass	Total scan subcutaneous adipose tissue (SAT) mass.	-
SAT Volume	Total scan subcutaneous adipose tissue (SAT) volume.	-
Total Lean Mass	Body composition total body lean mass.	Beneficial
Android Lean Mass	Body composition android lean mass.	Beneficial
Trunk Lean Mass	Body composition trunk lean mass.	Beneficial

References

[1] Lamont, R.J., Koo, H., Hajishengallis, G.: The oral microbiota: dynamic communities and host interactions. Nature reviews microbiology **16**(12), 745–759 (2018)

[2] Sharma, N., Bhatia, S., Sodhi, A.S., Batra, N.: Oral microbiome and health. AIMS microbiology **4**(1), 42 (2018)

[3] Jia, G., Zhi, A., Lai, P., Wang, G., Xia, Y., Xiong, Z., Zhang, H., Che, N., Ai, L.: The oral microbiota–a mechanistic role for systemic diseases. British dental journal **224**(6), 447–455 (2018)

[4] Baker, J.L., Mark Welch, J.L., Kauffman, K.M., McLean, J.S., He, X.: The oral microbiome: diversity, biogeography and human health. Nature Reviews Microbiology **22**(2), 89–104 (2024)

[5] Costalonga, M., Herzberg, M.C.: The oral microbiome and the immunobiology of periodontal disease and caries. Immunology letters **162**(2), 22–38 (2014)

[6] Tonelli, A., Lumngwena, E.N., Ntusi, N.A.: The oral microbiome in the pathophysiology of cardiovascular disease. Nature Reviews Cardiology **20**(6), 386–403 (2023)

[7] Levy, M., Kolodziejczyk, A.A., Thaiss, C.A., Elinav, E.: Dysbiosis and the immune system. Nature Reviews Immunology **17**(4), 219–232 (2017)

[8] Kuraji, R., Ye, C., Zhao, C., Gao, L., Martinez, A., Miyashita, Y., Radaic, A., Kamarajan, P., Le, C., Zhan, L., *et al.*: Nisin lantibiotic prevents nafld liver steatosis and mitochondrial oxidative stress following periodontal disease by abrogating oral, gut and liver dysbiosis. npj Biofilms and Microbiomes **10**(1), 3 (2024)

[9] Li, Y., Qian, F., Cheng, X., Wang, D., Wang, Y., Pan, Y., Chen, L., Wang, W., Tian, Y.: Dysbiosis of oral microbiota and metabolite profiles associated with type 2 diabetes mellitus. Microbiology spectrum **11**(1), 03796–22 (2023)

[10] Wang, T., Ishikawa, T., Sasaki, M., Chiba, T.: Oral and gut microbial dysbiosis and non-alcoholic fatty liver disease: the central role of porphyromonas gingivalis. Frontiers in medicine **9**, 822190 (2022)

[11] Huang, M., Zhang, X., Zhou, R., Song, Y., Zhang, J., Wu, J.: Advances in the study of oral microbiota and metabolism associated fatty liver disease: a systematic review. Frontiers in Cellular and Infection Microbiology **14**, 1491696 (2024)

[12] Hatipoğlu, Ö., Önsüren, A.S., Hatipoğlu, F.P., Kurt, A.: Caries-related salivary

parameters and oral microbial flora in patients with type 1 diabetes: A meta-analysis. Diabetes/Metabolism Research and Reviews **38**(5), 3527 (2022)

[13] Xiao, E., Mattos, M., Vieira, G.H.A., Chen, S., Corrêa, J.D., Wu, Y., Albiero, M.L., Bittinger, K., Graves, D.T.: Diabetes enhances il-17 expression and alters the oral microbiome to increase its pathogenicity. Cell host & microbe **22**(1), 120–128 (2017)

[14] Clarridge III, J.E.: Impact of 16s rrna gene sequence analysis for identification of bacteria on clinical microbiology and infectious diseases. Clinical microbiology reviews **17**(4), 840–862 (2004)

[15] Shilo, S., Bar, N., Keshet, A., Talmor-Barkan, Y., Rossman, H., Godneva, A., Aviv, Y., Edlitz, Y., Reicher, L., Kolobkov, D., *et al.*: 10 k: a large-scale prospective longitudinal study in israel. European journal of epidemiology **36**(11), 1187–1194 (2021)

[16] Visscher, P.M., Wray, N.R., Zhang, Q., Sklar, P., McCarthy, M.I., Brown, M.A., Yang, J.: 10 years of gwas discovery: biology, function, and translation. The American Journal of Human Genetics **101**(1), 5–22 (2017)

[17] Goh, C.E., Bohn, B., Marotz, C., Molinsky, R., Roy, S., Paster, B.J., Chen, C.-Y., Rosenbaum, M., Yuzefpolskaya, M., Colombo, P.C., *et al.*: Nitrite generating and depleting capacity of the oral microbiome and cardiometabolic risk: results from origins. Journal of the American Heart Association **11**(10), 023038 (2022)

[18] Zhao, F., Dong, T., Yuan, K.-Y., Wang, N.-J., Xia, F.-Z., Liu, D., Wang, Z.-M., Ma, R., Lu, Y.-L., Huang, Z.-W.: Shifts in the bacterial community of supragingival plaque associated with metabolic-associated fatty liver disease. Frontiers in Cellular and Infection Microbiology **10**, 581888 (2020)

[19] Vieira Lima, C.P., Pauletto, P., Lataro, R.M., De Luca Canto, G., Dame-Teixeira, N., Stefani, C.M.: The oral microbiome in diabetes, arterial hypertension, and obesity: A scoping review. Oral Microbiome: Symbiosis, Dysbiosis and Microbiome Interventions for Maintaining Oral and Systemic Health, 201–223 (2025)

[20] Lu, M., Xuan, S., Wang, Z.: Oral microbiota: A new view of body health. Food Science and Human Wellness **8**(1), 8–15 (2019)

[21] Monteiro, N.E., Roquetto, A.R., Pace, F., Moura, C.S., Dos Santos, A., Yamada, A.T., Saad, M.J.A., Amaya-Farfan, J.: Dietary whey proteins shield murine cecal microbiota from extensive disarray caused by a high-fat diet. Food Research International **85**, 121–130 (2016)

[22] Dong, T.S., Katzka, W., Lagishetty, V., Luu, K., Hauer, M., Pisegna, J., Jacobs, J.P.: A microbial signature identifies advanced fibrosis in patients with chronic

liver disease mainly due to nafld. Scientific reports **10**(1), 2771 (2020)

[23] Loomba, R., Seguritan, V., Li, W., Long, T., Klitgord, N., Bhatt, A., Dulai, P.S., Caussy, C., Bettencourt, R., Highlander, S.K., *et al.*: Gut microbiome-based metagenomic signature for non-invasive detection of advanced fibrosis in human nonalcoholic fatty liver disease. Cell metabolism **25**(5), 1054–1062 (2017)

[24] Komazaki, R., Katagiri, S., Takahashi, H., Maekawa, S., Shiba, T., Takeuchi, Y., Kitajima, Y., Ohtsu, A., Udagawa, S., Sasaki, N., *et al.*: Periodontal pathogenic bacteria, aggregatibacter actinomycetemcomitans affect non-alcoholic fatty liver disease by altering gut microbiota and glucose metabolism. Scientific reports **7**(1), 1–14 (2017)

[25] Gao, H., Wan, X., Xiao, B., Yang, K., Wang, Y., Zhang, C., Li, P., Liu, L., Xia, T., Wang, A., *et al.*: Impacts of pbde-47 exposure before, during and after pregnancy on the maternal gut microbiome and its association with host metabolism. Ecotoxicology and Environmental Safety **222**, 112530 (2021)

[26] Choi, J., Son, D., An, S., Cho, E., Lim, S., Lee, H.-J.: Effects of lactiplantibacillus plantarum cbt lp3 and bifidobacterium breve cbt br3 supplementation on weight loss and gut microbiota of overweight dogs. Scientific Reports **14**(1), 25446 (2024)

[27] Kim, H., Nelson, P., Nzabarushimana, E., Shen, J., Jensen, J., Bhosle, A., Li, C., Lee, N., Everett, C., Berdy, B., et al.: Multi-omic analysis reveals transkingdom gut dysbiosis in metabolic dysfunction-associated steatotic liver disease. Nature Metabolism, 1–17 (2025)

[28] Xu, Q., Wang, W., Li, Y., Cui, J., Zhu, M., Liu, Y., Liu, Y.: The oral-gut microbiota axis: a link in cardiometabolic diseases. npj Biofilms and Microbiomes **11**(1), 11 (2025)

[29] Favale, N., Farina, R., Carrieri, A., Simonelli, A., Severi, M., Sabbioni, S., Trombelli, L., Scapoli, C.: Functional profile of oral plaque microbiome: Further insight into the bidirectional relationship between type 2 diabetes and periodontitis. Molecular oral microbiology **39**(2), 62–79 (2024)

[30] Watanabe, K., Katagiri, S., Takahashi, H., Sasaki, N., Maekawa, S., Komazaki, R., Hatasa, M., Kitajima, Y., Maruyama, Y., Shiba, T., *et al.*: Porphyromonas gingivalis impairs glucose uptake in skeletal muscle associated with altering gut microbiota. The FASEB Journal **35**(2), 21171 (2021)

[31] Kashiwagi, Y., Aburaya, S., Sugiyama, N., Narukawa, Y., Sakamoto, Y., Takahashi, M., Uemura, H., Yamashita, R., Tominaga, S., Hayashi, S., *et al.*: Porphyromonas gingivalis induces entero-hepatic metabolic derangements with alteration of gut microbiota in a type 2 diabetes mouse model. Scientific reports **11**(1), 18398 (2021)

[32] Sedghi, L., DiMassa, V., Harrington, A., Lynch, S.V., Kapila, Y.L.: The oral microbiome: Role of key organisms and complex networks in oral health and disease. Periodontology 2000 **87**(1), 107–131 (2021)

[33] Zhao, Q., Yu, J., Zhou, H., Wang, X., Zhang, C., Hu, J., Hu, Y., Zheng, H., Zeng, F., Yue, C., *et al.*: Intestinal dysbiosis exacerbates the pathogenesis of psoriasis-like phenotype through changes in fatty acid metabolism. Signal Transduction and Targeted Therapy **8**(1), 40 (2023)

[34] Ebersole, J.L., Kirakodu, S.S., Zhang, X., Dawson III, D., Miller, C.S.: Salivary microbiome and biomarker characteristics of diabetics with periodontitis. Molecular Oral Microbiology **40**(1), 37–49 (2025)

[35] Ma, T., Huang, W., Li, Y., Jin, H., Kwok, L.-Y., Sun, Z., Zhang, H.: Probiotics alleviate constipation and inflammation in late gestating and lactating sows. npj Biofilms and Microbiomes **9**(1), 70 (2023)

[36] Park, H.-S., Song, J.-W., Park, J.-H., Lim, B.-K., Moon, O.-S., Son, H.-Y., Lee, J.-H., Gao, B., Won, Y.-S., Kwon, H.-J.: Txnip/vdup1 attenuates steatohepatitis via autophagy and fatty acid oxidation. Autophagy **17**(9), 2549–2564 (2021)

[37] Ram-Mohan, N., Meyer, M.M.: Comparative metatranscriptomics of periodontitis supports a common polymicrobial shift in metabolic function and identifies novel putative disease-associated ncrnas. Frontiers in Microbiology **11**, 482 (2020)

[38] Farley-Barnes, K.I., Baserga, S.J.: Ribosome biogenesis and its role in cell growth and proliferation in the liver. The Liver: Biology and Pathobiology, 174–182 (2020)

[39] Yang, S., Wang, L., Gao, R., Li, Y., Zhang, D., Wang, C., Liu, G., Na, J., Xu, P., Wang, X., et al.: Ufmylation safeguards human hepatocyte differentiation and liver homeostasis by regulating ribosome dissociation. Cell Reports **44**(5) (2025)

[40] Wang, J., Tang, H., Zhang, C., Zhao, Y., Derrien, M., Rocher, E., Vlieg, J.E., Strissel, K., Zhao, L., Obin, M., *et al.*: Modulation of gut microbiota during probiotic-mediated attenuation of metabolic syndrome in high fat diet-fed mice. The ISME journal **9**(1), 1–15 (2015)

[41] Kovatcheva-Datchary, P., Nilsson, A., Akrami, R., Lee, Y.S., De Vadder, F., Arora, T., Hallen, A., Martens, E., Björck, I., Bäckhed, F.: Dietary fiber-induced improvement in glucose metabolism is associated with increased abundance of prevotella. Cell metabolism **22**(6), 971–982 (2015)

[42] Zhao, L., Zhang, F., Ding, X., Wu, G., Lam, Y.Y., Wang, X., Fu, H., Xue, X., Lu, C., Ma, J., *et al.*: Gut bacteria selectively promoted by dietary fibers alleviate type 2 diabetes. Science **359**(6380), 1151–1156 (2018)

[43] Trammell, S.A., Brenner, C.: Targeted, lcms-based metabolomics for quantitative measurement of nad+ metabolites. Computational and structural biotechnology journal **4**(5), 201301012 (2013)

[44] Houtkooper, R.H., Cantó, C., Wanders, R.J., Auwerx, J.: The secret life of nad+: an old metabolite controlling new metabolic signaling pathways. Endocrine reviews **31**(2), 194–223 (2010)

[45] Zeybel, M., Altay, O., Arif, M., Li, X., Yang, H., Fredolini, C., Akyildiz, M., Saglam, B., Gonenli, M.G., Ural, D., *et al.*: Combined metabolic activators therapy ameliorates liver fat in nonalcoholic fatty liver disease patients. Molecular systems biology **17**(10), 10459 (2021)

[46] Vo, T., Merhej, V., Isber, C., Pontarotti, P., Bittar, F., Rolain, J.-M.: Global lessons from antibiotic resistance: metformin-hydrolyzing genes in transposable elements, a new threat for type ii diabetic patients? bioRxiv, 2025–04 (2025)

[47] Lan, X., Li, D., Zhong, B., Ren, J., Wang, X., Sun, Q., Li, Y., Liu, L., Liu, L., Lu, S.: Identification of differentially expressed genes related to metabolic syndrome induced with high-fat diet in e3 rats. Experimental biology and medicine **240**(2), 235–241 (2015)

[48] Zhou, Z., Sun, B., Huang, S., Jia, W., Yu, D.: The trna-associated dysregulation in diabetes mellitus. Metabolism **94**, 9–17 (2019)

[49] Wei, F.-Y., Tomizawa, K.: trna modifications and islet function. Diabetes, Obesity and Metabolism **20**, 20–27 (2018)

[50] Safi-Stibler, S., Thévenot, E.A., Jouneau, L., Jouin, M., Seyer, A., Jammes, H., Rousseau-Ralliard, D., Baly, C., Gabory, A.: Differential effects of post-weaning diet and maternal obesity on mouse liver and brain metabolomes. Nutrients **12**(6), 1572 (2020)

[51] Ruiz-Margáin, A., Macías-Rodríguez, R., Ríos-Torres, S., Román-Calleja, B., Méndez-Guerrero, O., Rodríguez-Córdova, P., Torre, A.: Effect of a high-protein, high-fiber diet plus supplementation with branched-chain amino acids on the nutritional status of patients with cirrhosis. Revista de Gastroenterología de México (English Edition) **83**(1), 9–15 (2018)

[52] Barber, C., Mego, M., Sabater, C., Vallejo, F., Bendezu, R.A., Masihy, M., Guarner, F., Espín, J.C., Margolles, A., Azpiroz, F.: Differential effects of western and mediterranean-type diets on gut microbiota: A metagenomics and metabolomics approach. Nutrients **13**(8), 2638 (2021)

[53] Park, H., Uhlemann, A., Jacobs, S., Mowbray, C., Jubelirer, T., Kelly, K., Walters, M., Ladas, E.: Obesogenic microbial signatures and the development of obesity in childhood acute lymphoblastic leukemia. Leukemia Research **126**, 107017 (2023)

[54] Zhu, Q., Jiang, S., Du, G.: Effects of exercise frequency on the gut microbiota in elderly individuals. Microbiologyopen **9**(8), 1053 (2020)

[55] Deepa Maheshvare, M., Raha, S., König, M., Pal, D.: A pathway model of glucose-stimulated insulin secretion in the pancreatic β-cell. Frontiers in endocrinology **14**, 1185656 (2023)

[56] Zahedi, K., Barone, S., Soleimani, M.: Polyamines and their metabolism: from the maintenance of physiological homeostasis to the mediation of disease. Medical Sciences **10**(3), 38 (2022)

[57] Choksomngam, Y., Pattanakuhar, S., Chattipakorn, N., Chattipakorn, S.C.: The metabolic role of spermidine in obesity: evidence from cells to community. Obesity Research & Clinical Practice **15**(4), 315–326 (2021)

[58] Wallace, M., Green, C.R., Roberts, L.S., Lee, Y.M., McCarville, J.L., Sanchez-Gurmaches, J., Meurs, N., Gengatharan, J.M., Hover, J.D., Phillips, S.A., *et al.*: Enzyme promiscuity drives branched-chain fatty acid synthesis in adipose tissues. Nature chemical biology **14**(11), 1021–1031 (2018)

[59] Shen, C., Chen, Y., Wang, Q., Sun, Y., Lin, H., Ni, M., Chen, Y., Zhang, L., Jin, J., Ying, X., *et al.*: Fecal short chain fatty acids modify therapeutic effects of sleeve gastrectomy. Frontiers in Endocrinology **14**, 1277035 (2023)

[60] Søndergård, S.D., Cintin, I., Kuhlman, A.B., Morville, T.H., Bergmann, M.L., Kjær, L.K., Poulsen, H.E., Giustarini, D., Rossi, R., Dela, F., *et al.*: The effects of 3 weeks of oral glutathione supplementation on whole body insulin sensitivity in obese males with and without type 2 diabetes: a randomized trial. Applied Physiology, Nutrition, and Metabolism **46**(9), 1133–1142 (2021)

[61] Dawi, J., Misakyan, Y., Affa, S., Kades, S., Narasimhan, A., Hajjar, F., Besser, M., Tumanyan, K., Venketaraman, V.: Oxidative stress, glutathione insufficiency, and inflammatory pathways in type 2 diabetes mellitus: Implications for therapeutic interventions. Biomedicines **13**(1), 18 (2024)

[62] Agarwal, P., Sampson, A., Hueneman, K., Choi, K., Jakobsen, N.A., Uible, E., Ishikawa, C., Yeung, J., Bolanos, L., Zhao, X., et al.: Microbial metabolite drives ageing-related clonal haematopoiesis via alpk1. Nature, 1–11 (2025)

[63] Lei, Y., Hu, H., Tang, H., Xu, L., Liu, R., Zhao, Y.: Homocysteine induces ferroptosis in renal tubular epithelial cells via β-catenin/gpx4 signaling pathway. Scientific Reports **15**(1), 23953 (2025)

[64] D'Aiuto, F., Gkranias, N., Bhowruth, D., Khan, T., Orlandi, M., Suvan, J., Masi, S., Tsakos, G., Hurel, S., Hingorani, A.D., *et al.*: Systemic effects of periodontitis treatment in patients with type 2 diabetes: a 12 month, single-centre, investigator-masked, randomised trial. The lancet Diabetes & endocrinology **6**(12), 954–965

(2018)

[65] Kamata, Y., Kessoku, T., Shimizu, T., Sato, S., Kobayashi, T., Kurihashi, T., Morozumi, T., Iwasaki, T., Takashiba, S., Hatanaka, K., *et al.*: Periodontal treatment and usual care for nonalcoholic fatty liver disease: a multicenter, randomized controlled trial. Clinical and Translational Gastroenterology **13**(11), 00520 (2022)

[66] Green, J., Green, S.J.: Topical prebiotic nitrate: can extending the 'hang-time'in the mouth improve oral-vascular health outcomes? npj Biofilms and Microbiomes **10**(1), 57 (2024)

[67] Broll, S., Urbanek, J., Buchanan, D., Chun, E., Muschelli, J., Punjabi, N.M., Gaynanova, I.: Interpreting blood glucose data with r package iglu. PloS one **16**(4), 0248560 (2021)